energies

MDPI

Article

Liquid CO_2 and Liquid Air Energy Storage Systems: A Thermodynamic Analysis

Matteo Marchionni [1,*] and Roberto Cipollone [2]

[1] Department of Mechanical, Chemical and Materials Engineering, University of Cagliari, Via Marengo, 2, 09123 Cagliari, Italy
[2] Department of Industrial and Information Engineering and Economics, University of L'Aquila, P.le Ernesto Pontieri, 1—Monteluco di Roio, 67100 L'Aquila, Italy; roberto.cipollone@univaq.it
* Correspondence: matteo.marchionni@unica.it; Tel.: +39-70-3248632406

Abstract: Energy storage is a key factor to confer a technological foundation to the concept of energy transition from fossil fuels to renewables. Their solar dependency (direct radiation, wind, biomass, hydro, etc. ...) makes storage a requirement to match the supply and demand, with fulfillment being another key factor. Recently, the most attention is directed toward the direct electrical storage inside batteries, probably driven by interest in the transportation sector, which today is the main focus in the transition path. On the contrary, for the generation of electrical energy and, more generally, for industrial sectors whose CO_2 emissions are defined as hard-to-abate, electrical storage is not a feasible answer to many political and non-technological concerns. Therefore, other storage methods must be considered to address excess electricity, the most characteristics of which being both the capacity and rate of charging/delivering. Among the efforts under consideration, the liquid storage of gases at ambient conditions is certainly an interesting option. This is the case with air and CO_2. The paper focused on the storage of CO_2 in liquid form, comparing its performance with those of air liquefaction, which well-studied in the literature. The paper proposed a novel plant layout design for a liquid CO_2 energy storage system that can improve the round-trip efficiency by up to 57%. The system was also compared to a liquid air energy storage unit considering a state-of-the-art level of technology for components, showing better efficiency but lower energy density. Finally, a sensitivity analysis was used to discuss the most relevant variables for a plant design. Particular focus was devoted to the discharging time of the plant, one of the most relevant variables that matches the energy demand.

Keywords: LCES; LAES; liquid carbon dioxide energy storage; liquid air energy storage; thermodynamic analysis; energy storage; parametric study

Citation: Marchionni, M.; Cipollone, R. Liquid CO_2 and Liquid Air Energy Storage Systems: A Thermodynamic Analysis. *Energies* **2023**, *16*, 4941. https://doi.org/10.3390/en16134941

Academic Editor: Alon Kuperman

Received: 22 May 2023
Revised: 21 June 2023
Accepted: 23 June 2023
Published: 25 June 2023

1. Introduction

The development of renewable energy systems (RES) is one of the main pillars in the strategy to accelerate the path toward the decarbonization of the economy and meet the climate-neutral targets agreed at the national and international levels. However, the intermittent, only partially predictable nature and fluctuating availability of renewable energy generation pose challenges in terms of grid management and stability as well as power availability. Energy storage, therefore, is an absolute need for the technological deployment of the new energy paradigm based on RES. Moreover, the use of energy storage technologies could also be beneficial for the improvement of the efficiency and operational flexibility of nuclear power plants, which represent another key alternative to achieve the abovementioned decarbonization objectives [1,2].

Although electro-chemical storage devices such as batteries and supercapacitors can help manage short-term fluctuations with superior efficiency, their short duration capacity, typically in the order of 6–8 h, and reduced lifetime [3], make them less suitable to cope with

the medium- and long-term fluctuations due, for instance, to the absence or lower intensity of solar radiation or wind speed in different weeks or seasons. The energy capacity of electro-chemical storage, as well, introduces some limits and necessitates the development of alternative options with long-term capabilities that can reduce the use of rare materials and the risks of political dependency. Moreover, the charging time strictly depends on the power of the charging stations; this requires specific infrastructures, intelligent reversible connections with the grid, safety aspects, proximity to the loads, endurance, and reliability for the charging–discharging cycles.

Chemical Storage (CS) is an interesting option based on the use of excess electricity generated by renewables to produce the so-called e-fuels or energy vectors, among which hydrogen is the most favorable candidate. CS is characterized by a large energy density and long-duration storage capacity. However, existing challenges for their development at larger scales include the low technology readiness level (TRL) of certain components as well as high costs of materials (i.e., electrolyzers for hydrogen production) [4,5].

Mechanical and thermo-mechanical storage (MS and TMS) are based on using excess electricity to store high-temperature thermal energy, mechanical potential energy, or mixed forms of energy. Among these options, pumped hydro-energy storage (PHES) presents higher values of roundtrip efficiency (70–80%) and higher TRL [6,7], but its development is subject to geographical constraints, requiring a natural storage site for water at heights above the ground level.

Compressed air energy storage (CAES) systems are also site-dependent [8], needing large natural caverns to store the air compressed with the excess electricity. This technology also requires additional heat input to increase the efficiency of the discharging phase and thus the overall roundtrip efficiency of the unit [8]. Furthermore, maintaining the gas at high pressures in such large geological volumes often presents challenges and requires additional energy consumption that negatively impacts the roundtrip efficiency. Compressed air leakages or diffusion across the surfaces, for instance, are the most important concerns which have no existing solution.

Pumped thermal energy storage (PTES) [9–14] is, on the contrary, independent of the geographical location and site, but its efficiency is limited by the coefficient of performance (COP) achievable during the conversion of the excess electricity into thermal power, which occurs in the charging stage. Additionally, the temperature at which such thermal power is stored also impacts the roundtrip efficiency of the overall plant. The temperature level constrains the efficiency of the thermal engine, which converts the heat back to electricity during the discharging stage.

A promising alternative is represented by liquid air energy storage (LAES) systems, which use electricity generated by renewables to liquefy air that is eventually vaporized, heated, and expanded during the discharging phase [15]. This will happen during nighttime or the peak periods of electricity demands. LAES systems are an evolution of CAES, and liquefying air can substantially increase the energy storage density and thus solve the site dependency by reducing the footprint of the plant [16]. LAES roundtrip efficiency is expected to be in the order of 50–60% [17]. The limiting aspect for the efficiency of LAES systems is the air compression process at high pressure, which is thermodynamically more energy intensive compared to other storage systems. In reality, a trade-off between energy stored and energy consumption is a key factor.

For these reasons, which do not address a more suitable energy storage system, recently, some researchers have tried to investigate the use of CO_2 as a working fluid for energy storage, namely liquid or compressed CO_2-based energy storage (LCES or CCES) [18,19]. The higher density of CO_2 at ambient pressure allows a more efficient compression [20,21] and therefore a potentially higher roundtrip efficiency [22]. Similarly to CAES and LAES, CCES or LCES compress CO_2 with excess electricity at high pressure under gaseous or liquid forms. Such systems usually operate in a closed-loop form since the processed CO_2 cannot be released into the atmosphere. Therefore, huge volumes are

needed to manage the CO_2 in the gaseous form that is required to operate the plant [22] during the discharge phase.

Some authors have studied such technology, foreseeing artificial domes [22], pools [23], natural caverns [24], or dismissed mines [25] to capture and sequestrate the CO_2 after the discharging phase. Others have considered using supercritical CO_2 along the whole charging and discharging phase to reduce the required volumes, but the reduced pressure ratio available limited the achievable roundtrip efficiency to 39% [26].

Performance analysis and the design of the different components required for a liquid carbon dioxide storage system were also carried out and reported in [14] with promising results in terms of roundtrip efficiency (around 64%) thanks to the integration of waste heat sources. In any case, LAES and LCES/CCES systems appear to be the most probable candidates for long-term energy storage.

Despite the available works in the literature on the thermodynamic analysis of the abovementioned systems, the reported results typically differ because of the different assumptions considered both on the modeling methodology as well as components' performance parameters. This prevents a rigorous comparison between such technologies and the respective potential advantages.

To fill this gap, a thermodynamic analysis was carried out by comparing a standard LAES system with a particular configuration of an LCES unit considering similar assumptions for the isentropic efficiency of turbomachines, pinch points in heat exchangers, and electro-mechanical efficiency of motors and generators. For the analysis, the thermal input given by the combustion of natural gas was considered for the two different types of systems. The performance and energy density of the two types of plants were analyzed and discussed. The particular LCES configuration presented not only achieved higher roundtrip efficiency but also reduced the volumes required for the storage of the working fluid. Finally, a sensitivity analysis was carried out to further optimize the system configuration and the key thermodynamic parameters.

2. Modelling Methodology

The development of the thermodynamic model of the two systems was carried out using MATLAB®. The model was used to perform a first and second law steady-state analysis, using CoolProp [27] for the calculation of the thermo-physical properties of the different fluids involved. Pinch points and energy balance equations were used to calculate the temperature of the different streams at the outlet of heat exchangers. To account for the changing thermo-physical properties of the CO_2, especially outside the ideal gas region, the heat exchangers were modeled considering a spatial-steady one-dimensional discretization. Thermal losses along pipes and in the thermal storage tanks were neglected, as well as the pressure drops across heat exchangers. The auxiliary power required by the different pumps for the circulation of the several fluids involved in the processes was neglected owing to their limited effect on the overall round-trip efficiency of the plant.

The governing equations for the first-principle analysis are the steady-state mass and energy balances. In particular, for each component of the system, Equations (1) and (2) apply:

$$\dot{m}_{in} = \dot{m}_{out} \tag{1}$$

$$\dot{m}_{hs}(h_{in} - h_{out}) = \dot{m}_{cs}(h_{in} - h_{out}) \tag{2}$$

where the subscripts *in* and *out* are, respectively, the inlet and outlet of a generic component, and *hs* and *cs* are the hot side and cold side of a generic heat exchanger. The thermal input given by the combustion of the natural gas can be calculated using the lower heating value (*LHV*) of the fuel, as shown in Equation (3).

$$\dot{Q}_{in} = \dot{m}_{CH_4} LHV \tag{3}$$

As concerns the turbomachines, isentropic efficiency and temperatures at the inlet of the machine are the input data as well as the maximum pressure of the different cycles of the two energy storage systems. Hence, enthalpy at the turbine, compressors, and pump outlets are computed through Equations (4)–(6), respectively, while for the temperature at the machine outlets Equation (7) applies.

$$h_{T,out} = h(p_{in}, s_{in}) - (h(p_{in}, s_{in}) - h(p_{out}, s_{in}))\eta_{T,is} \quad (4)$$

$$h_{C,out} = h(p_{in}, s_{in}) + (h(p_{out}, s_{in}) - h(p_{in}, s_{in}))/\eta_{C,is} \quad (5)$$

$$h_{PMP,out} = h(p_{in}, s_{in}) + (h(p_{out}, s_{in}) - h(p_{in}, s_{in}))/\eta_{PMP,is} \quad (6)$$

$$T_{out} = T(p_{out}, h_{out}) \quad (7)$$

In those cases when reheating and intercooling are considered, the optimal pressure ratio across the machines has been calculated with Equation (8):

$$PR_i = \sqrt[NS]{(p_{max}/p_{min})} \quad (8)$$

where PR_i is the pressure ratio across the i-th turbomachine, p_{max} and p_{min} are the maximum and minimum pressure respectively across the compressor/turbine train and NS is the number of compression/expansion stages considered.

The electrical power produced by the turbines or required by the compressors or pumps is calculated using Equations (9)–(11). The parameters η_m and η_{el}, whose values are reported in Table 1, refer to the mechanical and electrical efficiencies of the motor/generator.

$$\dot{W}_T = \dot{m}_T(h_{T,in} - h_{T,out})\eta_m\eta_{el} \quad (9)$$

$$\dot{W}_C = \dot{m}_C(h_{C,out} - h_{C,in})/\eta_m\eta_{el} \quad (10)$$

$$\dot{W}_{PMP} = \frac{\dot{m}_{PMP}(h_{PMP,out} - h_{PMP,in})}{\eta_m\eta_{el}} \quad (11)$$

Table 1. Assumptions for the parameters used in the analysis.

	Unit	LAES	LCES
Power size	MW	50	
Charge time	hours	8	
Generator efficiency	%	95	
Mechanical efficiency	%	98	
Turbines			
Isentropic efficiency	%	89	85
Inlet temperature	°C	1300	1000
Inlet pressure	bar	22	250
Discharge pressure	bar	1	20
Number of stages	#	1	
Compressors			
Isentropic efficiency	%	85	80
Inlet temperature	°C	1	−14
Inlet pressure	bar	1	5.2
Maximum pressure	bar	125	250
Number of stages	#	3	
Heat Exchangers (HXs)			
Pinch point	°C	15	
Combustors	#	1	
Number of HXs	#	8	8
Intercoolers	#	3	

The electric power during the discharge and charging stage, as well as the overall roundtrip efficiency of the cycle, are calculated as in Equations (12)–(14):

$$\dot{W}_{disch} = \sum_{j}^{NT} W_{T,j} \tag{12}$$

$$\dot{W}_{ch} = \sum_{i}^{NC} W_{C,i} + \sum_{z}^{NPMP} W_{PMP,z} \tag{13}$$

$$\eta_{RT} = \frac{\dot{W}_{disch} t_{disch}}{\dot{W}_{ch} t_{ch} + \dot{Q}_{in} t_{disch}} \tag{14}$$

where t_{ch} and t_{disch} are the charging and discharging time, while *NT*, *NC*, and *NPMP* are, respectively, the number of turbines, compressors, and pumps installed in each layout.

For the exergy analysis, assuming a dead state at ambient conditions (1 bar, 15 °C), exergy flows for each stream in each component are calculated as per Equation (11):

$$\dot{E}_i = \dot{m}_i (h_i - T_0 s_i) \tag{15}$$

and the exergy irreversibility for heat exchangers, turbines, compressors, pumps, and combustors can be evaluated through Equations (16)–(20):

$$\dot{I}_T = \dot{E}_{T,in} - \dot{W}_T - \dot{E}_{T,out} \tag{16}$$

$$\dot{I}_C = \dot{E}_{C,in} + \dot{W}_C - \dot{E}_{C,out} \tag{17}$$

$$\dot{I}_{PMP} = \dot{E}_{PMP,in} + \dot{W}_{PMP} - \dot{E}_{PMP,out} \tag{18}$$

$$\dot{I}_{HX} = \dot{E}_{cs,in} - \dot{E}_{cs,out} + \dot{E}_{hs,in} - \dot{E}_{hs,out} \tag{19}$$

$$\dot{I}_{CC} = \dot{m}_{CH_4} LHV + \dot{E}_{in} - \dot{E}_{out} \tag{20}$$

3. Selected Configurations

The analyzed LAES configuration is an advanced layout taken from the literature [28], while the LCES system differs from the layouts studied previously in the literature because allows the storage of the CO_2 in liquid form at the end of both the charging and the discharging cycle. At the same time, the maximization of the pressure ratio across the turbine during the discharging phase was considered. This particular arrangement was devised to improve the energy density of LCES systems. Both systems (LAES and LCES) consider the combustion of a fuel to increase the temperature of the fluid expanded in the turbine during the discharging phase. Although the LAES system implements direct combustion, in the LCES unit, the CO_2 is heated indirectly with the heat provided by the combustion of a fuel.

Even if the fuel considered for this study is natural gas, for the CO_2 case (indirect combustion), an alternative fuel such as hydrogen or a bio-fuel or blends could be used to avoid the use of a fossil fuel. In both cases, the electro-mechanical efficiency of the turbomachines was taken into account to compute the electrical power absorbed and released during the charging and discharging phases, respectively. Table 1 reports the power scale and the charging time assumed for the two systems together with other parameters related to the main plant components. The temperature at the inlet of the turbines as well as the isentropic efficiency for compressors and turbines were assumed considering state-of-the-art components [29,30].

The temperature at the turbine inlet for the two different systems was purposely assumed as different. These values were selected based on the current limitations of state-of-the-art air and CO_2 turbines. While in modern gas turbines it is reasonable to assume an inlet temperature of 1300 °C, for CO_2 turbines, whose technology is less mature, we

decided to consider a lower value, equal to 1000 °C. In the same fashion, for the LCES case, a lower value of the isentropic efficiency was also considered for both the compressor and turbine [29,30]. As intermediate heat transfer fluid used in intercoolers and coolers, pressurized water was considered for both systems.

3.1. LAES

The LAES system configuration is shown in Figure 1 and realized the Hampton–Linde air liquefaction process [31]. During the charging process, the air was compressed by a train of three intercooled compressors and cooled down by a third intercooler (IC3). The heat recovered by the water in the intercoolers was stored in a TES system, which was consequently used for heating the air stream in the discharging phase. After the intercooler IC3, the air was cooled to the temperature of −183 °C in a multi-stream heat exchanger, namely the Coldbox (CB), using two fluids, i.e., methanol and propane.

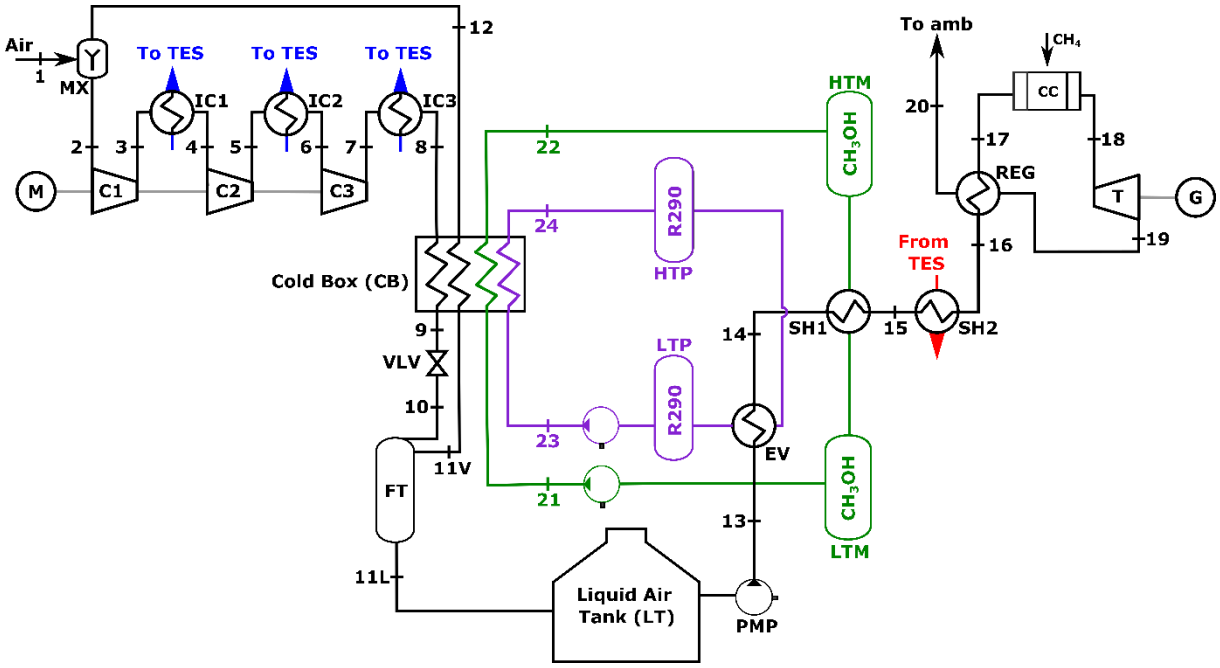

Figure 1. Layout of the LAES system.

In the initial phase of the charging cycle, such fluids were stored at low temperatures (−185 °C for propane and −60 °C for methanol) in two cryogenic tanks (LTP and LTM, Figure 1) and used as a heat sink in the Coldbox. Afterward, the Coldbox air was laminated in an expansion valve (VLV) down to a pressure of 1.5 bar (point 10) and directed in a flash tank (FT) where the liquid and vapor phases were separated. The liquid air at saturated conditions was stored in a tank (LT) while the saturated vapor (point 11V) was recycled in the Coldbox to provide additional cooling to the air stream coming from the compressor (point 8). This vapor stream, at the outlet of the Coldbox, was sent to a mixer (MX) upstream of the first compressor (C1), lowering the air inlet temperature and thus reducing the mechanical work required for the compression itself.

The propane and methanol fluid used to cool down the air stream during the charging phase were then stored in two high-temperature tanks (HTP and HTM in Figure 2) at −60 °C and 25 °C, respectively.

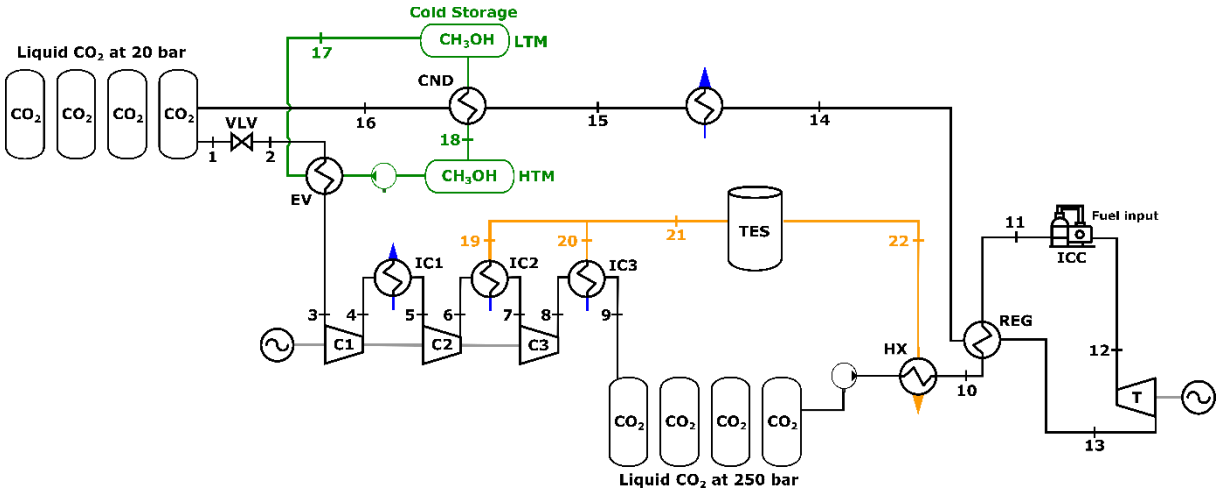

Figure 2. Layout of the LCES system.

During the discharging phase, the air was pressurized in the pump (PMP) up to a pressure of 22 bar, evaporated in the heat exchanger (EV), and superheated up to 15 °C in the first superheater (SH1). During the evaporation, the propane was cooled back to −185 °C while the methanol was cooled down in the SH1 to −60 °C. The fluids were then stored in the low-temperature tanks (LTP and LTM).

After the superheating in the heat exchanger SH1, the air stream first was heated in the second superheater (SH2) by the thermal energy stored in the TES system during the charging stage, and then heated in the regenerator (REG). The air was further heated by the combustion of the natural gas in the combustor (CC) and then expanded in the turbine (T). After the expansion, the flue gas stream was rejected into the environment after transferring its residual heat to the stream coming from the superheater SH2 in the regenerator (REG). Table 2 shows the calculated thermodynamic conditions of the air in the different points reported in Figure 1 as well as the mass flow rates of the different fluids. Table 3 shows the temperature, pressure, and mass flow rates of water in the different intercoolers and the heat exchanger SH2. The thermodynamic calculations were in good agreement with a similar LAES system analyzed in [28] and differ for the mass flow rates processed because of the different power scales considered.

Table 2. Thermodynamic calculation for the LAES system (point numbers refer to Figure 1).

Point	Pressure (bar)	Temperature (°C)	Mass Flow Rate (kg/s)
Air			
1	1	15	69.4
2	1	1	76.9
3	5	180	76.9
4	5	25	76.9
5	25	228	76.9
6	25	25	76.9
7	125	230	76.9
8	125	25	76.9
9	125	−50	76.9
10	125	−183	76.9
11L	1	−191	69.4
11V	1	−191	7.7
12	1	−130	7.7
13	22	−190	76.9
14	22	−111	76.9
15	22	−23	76.9

Table 2. *Cont.*

Point	Pressure (bar)	Temperature (°C)	Mass Flow Rate (kg/s)
16	22	180	76.9
17	22	365	76.9
18	22	1000	76.9
19	1	375	78.2
20	1	186	78.2
Methanol			
21	2	−60	46
22	2	15	46
Propane			
23	3	−185	224.5
24	3	−60	224.5

Table 3. Temperature, pressure, and mass flow rate of water streams at the inlet (in) and outlet (out) of intercoolers (IC1, IC2, and IC3) as well as the heat exchanger (SH2).

Heat Exchanger		IC1	IC2	IC3	SH2
Pressure in	bar		10		
Mass flow rate	kg/s	45.0	57.3	62.3	62.3
Temperature in	°C		15		160
Temperature out	°C		160		15

3.2. LCES

The LCES layout proposed is shown in Figure 2. Contrarily to the LAES system, it uses CO_2 as a working fluid instead of air, and therefore it is a closed loop. For this reason, two sets of tanks at two different pressure levels are foreseen to collect the CO_2 at the end of the charging and discharging phase, since the CO_2 cannot be rejected into the environment in such large quantities. At the beginning of the charging phase, the CO_2 is stored in cryogenic tanks at a pressure of 20 bar in saturated liquid conditions.

Once the charging phase starts, according to the layout shown in Figure 2, the CO_2 expanded from the tank at the low pressure of 20 bar down to 5.2 bar (point 2, upstream the evaporator EV) owing to a laminating valve (VLV). Downstream the valve (point 2), the CO_2 was in two-phase conditions, and therefore the remaining liquid CO_2 evaporated in the heat exchanger EV and was slightly superheated before flowing into the compressor. During the evaporation, a stream of methanol cooled down to −53 °C and was stored in a cryogenic tank (LTM). Such fluid was used during the discharging phase to condensate back the CO_2 in liquid form after the expansion in the Condenser (CND in Figure 2). Because the heat required during the evaporation of the CO_2 at a pressure of 5.2 bar is higher than the one required for the CO_2 condensation at 20 bar, the mass flow rate of methanol used was only equal to the value required during the discharging phase. The rest of the thermal power was provided by ambient air. This arrangement allowed reducing the overall volume required for the storage of the methanol.

Once in the vapor state, the CO_2 stream was compressed and intercooled in the compressor train (C1, IC1, C2, IC2, C3) up to 250 bar and then cooled down in the cooler (IC3) to be stored in the high-pressure CO_2 tanks at ambient temperature.

The heat transferred from the CO_2 to the water in the three intercoolers was recovered and stored in a thermal energy storage system to be re-used during the discharging phase to heat up the CO_2 in the heat exchanger HX up to a temperature of 118 °C (point 10). After this first heating stage, the CO_2 was indirectly heated in the regenerator and in the combustor up to a temperature of 1000 °C. Downstream of the indirect combustor (ICC), the high-temperature and high-pressure CO_2 stream expanded in the turbine (T) down to the discharge pressure of 20 bar (point 13 in Figure 2). The residual heat of the CO_2 at the

turbine outlet was used to heat the stream at point 10 in the regenerator (REG). Downstream of the regenerator, the CO_2 stream was cooled down to ambient temperature in the heat exchanger (COOL) and finally liquefied in the condenser (CND) owing to the stream of cold methanol flowing from the low-temperature tank (LTM) to the high-temperature tank (HTM) placed downstream of the condenser (point 18 in Figure 2). The indirect combustion, despite being slightly less efficient than the direct one occurring in LAES systems, allows the usage of alternative fuels such as hydrogen, e-fuels, or biomass-derived gas.

Furthermore, the use of CO_2 as a working fluid could potentially allow performing the heating stage of the fluid in an oxycombustor rather than with indirect combustion. As a following advantage, the costs for a carbon capture and storage system would be reduced and the overall efficiency of the system increases [32]. Table 4 reports the calculated thermodynamic conditions and the mass flow rates of the different streams in the points depicted in Figure 2.

Table 4. Thermodynamic data of the LCES system.

Point	Pressure (bar)	Temperature (°C)	Mass Flow Rate (kg/s)
Air			
1	20.0	−19	214.0
2	5.2	−56	214.0
3	5.2	−51	214.0
4	18.9	45	214.0
5	18.9	25	214.0
6	68.7	145	214.0
7	68.7	35	214.0
8	250.0	141	214.0
9	250.0	15	214.0
10	250.0	118	103.4
11	250.0	530	103.4
12	250.0	1000	103.4
13	20.0	635	103.4
14	20.0	128	103.4
15	20.0	25	103.4
16	20.0	−19	103.4
Methanol			
17	2	−53	335
18	2	−22	335
Water			
19	6	130	71.2
20	6	126	112.4
21	6	128	185.6
22	6	128	116.0

3.3. Performance Comparison and Exergy Analysis

In the analysis of both systems, the electric power provided during the discharging phase was assumed equal to be 50 MW, equal to the amount absorbed during the charging phase. The calculations related to the performance of the two units are reported in Table 5. We observed that the LCES compressors, owing to the higher density of CO_2, and therefore the reduced mechanical power required for the compression, can store a higher amount of fluid in the same charge time of 8 h.

Table 5. Performance of the LAES and LCES system.

	Unit	LAES	LCES
Input			
Power discharge	MW	50	
Charge time (input)	hours	8	
Output			
Discharge time	hours	7.2	14.6
C-to-D ratio	-	0.9	1.8
Roundtrip efficiency	%	46.3	50.0
Fuel consumption	kg/MWh	205	121
Heat available	GWh/cycle	89.0	91.1

This results in a higher amount of energy released during the discharging stage and therefore a longer discharge time compared to the LAES system, 14.6 h against 7.2 h (Table 5), with a double charge-to-discharge (C-to-D) time ratio (1.8 against 0.9, Table 5). The longer discharge time is a strong advantage for energy storage systems, since it allows higher operational flexibility in coping with RES power supply fluctuations as well as the possibility to sustain a longer electric load.

The LCES plant also showed a higher roundtrip efficiency, equal to 50.0%, against 46.3% of LAES. The slightly lower efficiency obtained for the LAES system compared to the literature is due to the consideration of the efficiency of the electro-mechanical energy conversion process in the analysis.

Because of the higher amount of fluid stored and the more efficient charging/discharging cycle, the fuel consumption of the LCES system per MWh of energy discharged was much lower, i.e., 121 kg/MWh against the consumption of 205 kg/MWh of fuel in the LAES case.

The analysis also showed that the LCES system had 91.1 GWh/cycle of unused thermal energy (recovered from cooling water) available at 128 °C that could be exploited, eventually with an ORC-based recovery unit, to increase further the roundtrip efficiency of the system. The LAES on the contrary had a slightly lower amount of unused heat, 89.0 GWh/cycle, but available at a higher temperature of 160 °C.

Table 6 shows the required calculated volumes for the different fluids used by the two plants. Because the LCES allows storing higher amount of fluids during the charging phase and is a closed-loop system, the volumes required to store the working fluid are approximately double that of the ones needed by the LAES plant. The volumes required for the storage of the cryogenic liquid are also higher in the LCES case, mainly because of the small temperature difference between the CO_2 condensation and evaporation at 20 bar and 5.2 bar, respectively. This requires large mass flow rates of methanol to cool down and heat the fluid and therefore large storage volumes. For this reason, the LAES system showed a higher energy density compared to LCES one, namely, 21 kWh/m^3 against 15 kWh/m^3 (Table 6).

Table 6. Volumes of fluids required from the analyzed LAES and LCES systems.

Volumes	Unit	LAES	LCES
Working fluid	m^3	2500	12,000
Hot water	m^3	2200	5000
Methanol	m^3	3500	33,000
Propane	m^3	9100	-
Total	m^3	17,300	50,000
Energy density	kWh/m^3	21	15

The results of the exergy analysis are shown in Tables 7 and 8. In particular, Table 7 shows the exergy destruction occurring in the different components of the LAES system

for each charge/discharge cycle and are expressed in MWh/cycle. Among the different components, the combustor showed a higher exergy destruction of 267.9 MWh/cycle, followed by the first superheater SH1, the evaporator, and the expansion valve (Table 7). The expansion valve irreversibility is due to the large pressure differential across the component, which, however is required to obtain a small vapor quality at its outlet to not excessively compromise the efficiency of the overall process. Increasing the vapor quality at the outlet of the expansion valve would increase the mass flow rate of air recirculated by the compressors and prevent liquefication, thus decreasing the roundtrip efficiency of the system.

Table 7. Exergy destruction for the different components of the LAES plant.

Component	Notation	Exergy Destruction
		MWh/cycle
Compressor 1	C1	11.2
Compressor 2	C2	3.9
Compressor 3	C3	11.3
Intercooler 1	IC1	9.4
Intercooler 2	IC2	11.4
Intercooler 3	IC3	10.0
Coldbox	CB	8.2
Expansion valve	VLV	30.9
Pump	PMP	1.9
Evaporator	EV	36.2
Superheater 1	SH1	41.8
Superheater 2	SH2	4.0
Regenerator	REG	2.6
Combustor	CC	124.0
Turbine	T	20.9
Total		328.0
Exergy unitary loss		0.9 MWh/MWh

Table 8. Exergy destruction for the different components of the LCES plant.

Component	Notation	Exergy Destruction
		MWh/cycle
Expansion valve	VLV	0.8
Evaporator	EV	53.4
Compressor 1	C1	23.1
Compressor 2	C2	22.6
Compressor 3	C3	16.0
Intercooler 1	IC1	1.4
Intercooler 2	IC2	6.8
Intercooler 3	IC3	11.8
Heater	HX	10.0
Regenerator	REG	56.6
Combustor	ICC	291.7
Turbine	T	31.6
Cooler	COOL	5.2
Condenser	CND	53.7
Total		584.9
Exergy unitary loss		0.8 MWh/MWh

For the evaporator and the superheater SH1, the higher losses are due to the evaporation of air. A possible solution to improve the efficiency of the process would be performing the heating of the fluid in supercritical conditions, which, however would require higher

pressure at the outlet of the air-liquid pump (over 34 bar, the air critical pressure), increased heat exchanger heat transfer area, and additional stages in the turbine to process a larger pressure ratio across the machine.

The irreversibility in the Coldbox was instead quite limited owing to the good thermal matching of the different streams in the heat exchanger and to the additional cooling provided by the amount of non-liquefied air at the outlet of the expansion valve which was recirculated. The same low exergy destruction rate occurred in components such as the regenerator, the intercoolers, and the second superheater SH2. Indeed, such components process fluids with similar thermophysical properties along the whole heat exchanger surface, which allows better thermal matching and therefore reduced exergy destruction. Table 7 also reports the overall exergy loss for the LAES plant per MWh of electrical energy stored in each charge–discharge cycle.

Table 8 shows the exergy destruction occurring in the LCES plant components. Even in this case, the indirect combustor (ICC) showed the highest irreversibility, equal to 291.7 MWh/cycle. It is possible to see that the condensation and evaporation process, required to have the CO_2 at the liquid and gas phase at the end and the beginning of the discharging and charging stage, respectively, also represents a large source of losses. These processes are unavoidable, however, when performing CO_2 storage in liquid form.

The third compressor had a much lower irreversibility than the first two because it operated closer to the critical point, allowing a further increase the of efficiency of the compression. Among the intercoolers, on the contrary, it was the first one presenting a reduced exergy destruction rate, mainly because of the lower mass flow rate of water required due to the lower temperature of 45 °C at the first compressor outlet. The third intercooler presented a larger irreversibility due to the higher mass flow rate of water required to cool down the CO_2 close to the critical point.

In general, the analysis showed that the overall exergy loss occurring in the LCES plant, equal to 584.9 MWh/cycle, was higher than the one in the LAES unit, equal to 328.0 MWh/cycle, due to larger mass flow rates circulating in the system and therefore greater exergy destruction in heat exchangers and turbomachines. Despite the exergy loss in absolute terms is higher in the LCES case, the unitary exergy loss, calculated as the total exergy destruction over the energy released during the discharging phase, was lower, being equal to 0.80 MWh/MWh against the 0.9 MWh/MWh of the LAES unit (Tables 7 and 8).

Figure 3 compares the relative exergy destruction rates of the components for both systems, calculated as the exergy destruction rate in the component over the exergy loss in the plant. The irreversibilities are grouped according to the typology of the component. The main noticeable differences relate to the following:

- The combustion represented the major source of losses for both units, representing 39% and 42% of the overall exergy loss for the LAES and LCES, respectively. The higher exergy losses in the LCES combustor are due to indirect combustion, less efficient than in the direct one;
- The LCES compressors also presented higher losses because of the higher mass flow rates processed, almost triple that of the LAES system, and a slightly lower isentropic efficiency of the CO_2 compressors due to the less mature technology of such turbomachines;
- While exergy losses in LAES intercoolers are almost comparable, the LCES one differed depending on the intercooler considered mainly because of the different thermodynamic conditions of the CO_2 at the inlet of the three compressors;
- The expansion in the lamination valve of the LAES system led to greater irreversibilities than the one occurring in the LCES unit due to the much larger expansion ratio across the component required to avoid an excessive vapor quality at the inlet of the flash tank;
- The regenerator had a larger impact on the overall exergy destruction of the plant. This is due to the thermo-physical properties of the CO_2. In fact, on the high-pressure side of the regenerator, the CO_2 was closer to the supercritical area and had a higher heat

capacity than the fluid at the low-pressure side flowing out from the turbine. For this reason, the regeneration was less efficient than the air regeneration occurring in the LAES plant, where both streams had similar heat capacities and densities. A possible solution to improve such heat transfer would be the adoption of a more complex layout allowing the split of the regeneration process in two different heat exchangers and then a better thermal matching of the CO_2 streams, with a consequent reduction of exergy losses. This would allow having a higher CO_2 temperature downstream the high-pressure side of the regenerator (point 11 in Figure 2) and then a reduction of the thermal input from the natural gas combustion, with a consequent reduction of fuel consumption;

- The higher exergy loss occurring in the CO_2 evaporator is also due to the larger mass flow rate of CO_2 processed during the system charging stage;
- Despite the larger number of components of the LAES system, in absolute terms, the exergy loss in the LCES plant was higher. However, increasing the number of heat exchangers in the LCES plant could lead to a more efficient heat transfer and thus in a reduction of the irreversibilities.

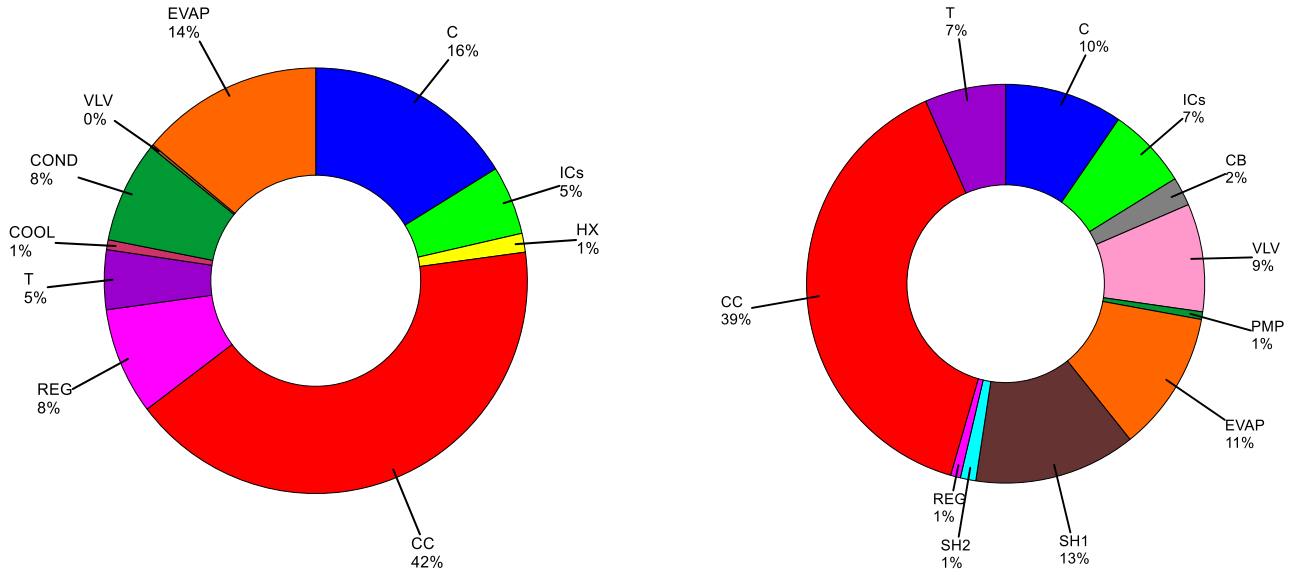

Figure 3. Exergy destruction comparison by component typology for the LAES (**a**) and LCES (**b**) system.

4. LCES Parametric Analysis

The comparison showed that LAES systems present a higher energy density compared to the LCES layout proposed, which, however, showed higher roundtrip efficiency. For this reason, a parametric analysis was carried out to understand how to further optimize the performance of the LCES plant and try to maximize the energy density indicator. For this purpose, four key system parameters were considered: the temperature at the turbine inlet, the maximum storage pressure of the CO_2, the discharge pressure at the turbine outlet, and the number of reheaters considered in the plant. Although the first three are thermodynamic variables, the latter relates to the system layout. The range of the parameter's variations is reported in Table 9. For each set of simulations, one thermodynamic parameter was singularly varied together with the number of reheating stages while keeping the other ones equal to their respective reference (ref) values (Table 9). For the discharge pressure of the unit, a minimum value of 10 bar was selected since it is the lowest pressure at which would be possible to close the charge–discharge cycle having the CO_2 still in the liquid phase. For the turbine inlet temperature, a maximum value of 1300 °C was selected to take into account future developments and progress in component technology.

Table 9. Range of values, minimum (min), reference (ref) and maximum (max), used for the parametric analysis for the key variables changed.

Parameter	Unit	Min Value	Ref Value	Max Value
Turbine inlet temperature	°C	700	1000	1300
Maximum pressure	bar	125	250	250
Discharge pressure	bar	10	20	40
Number of reheating stages	#	0	0	2

Figure 4 shows the results of the analysis related to the change in the turbine inlet temperature. In particular, the effect of this parameter on the roundtrip efficiency, the energy density, the fuel consumption over the discharging cycle, and the discharge time achievable were considered. In this work, the concept of roundtrip efficiency was calculated as the electricity generated in the discharging phase over the renewable energy stored during the fluid compression plus the thermal energy input introduced with the combustion of methane. It did not consider uniquely the energy stored from renewable sources, even if the methane could be produced from bio-mass or substituted with green hydrogen.

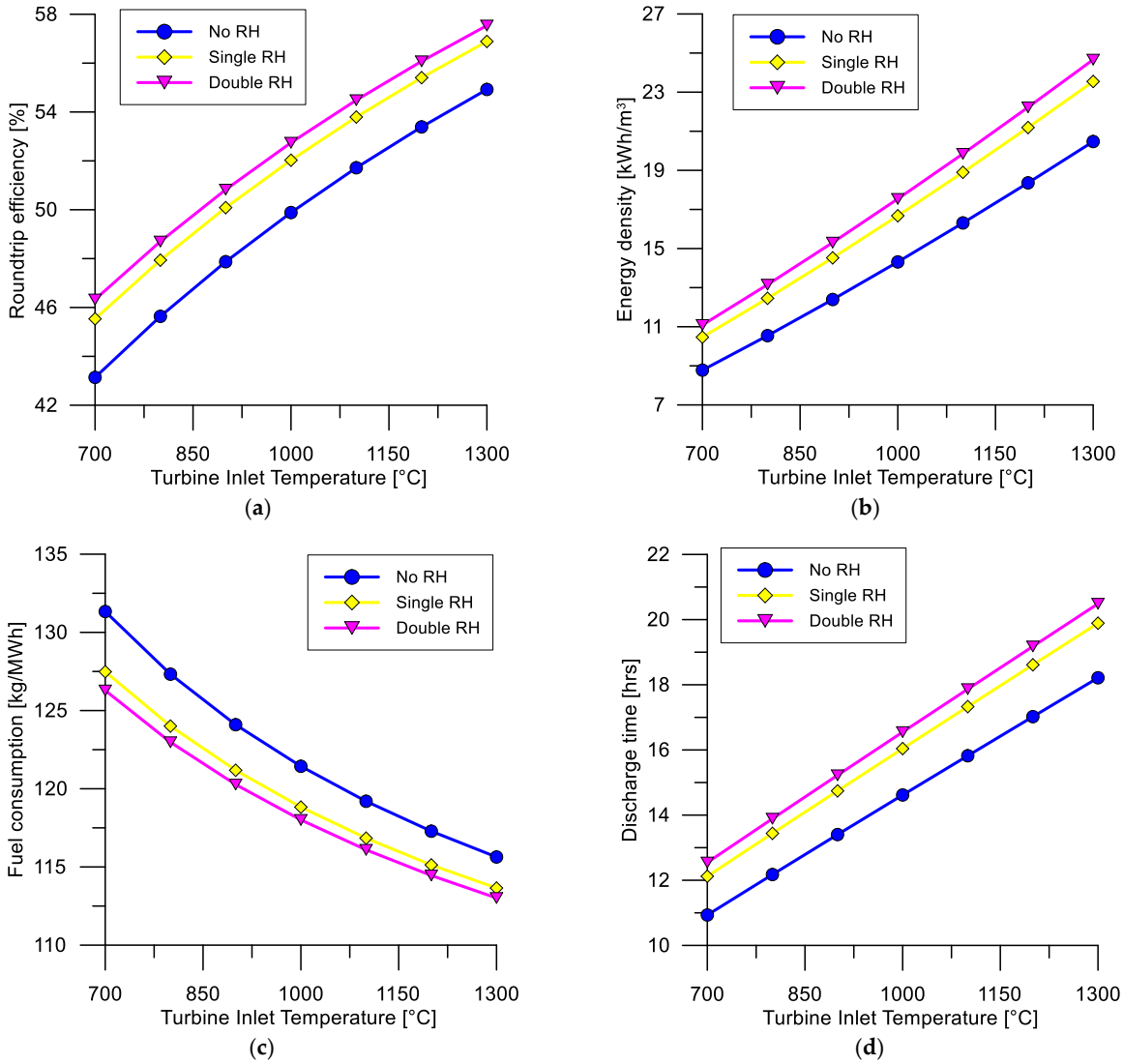

Figure 4. Effect of the turbine inlet temperature and number of reheaters (RH) on the LCES system roundtrip efficiency (**a**), energy density (**b**), fuel consumption during a discharge cycle (**c**), and discharge time (**d**).

Figure 4a shows the positive effect of the turbine inlet temperature on the roundtrip efficiency, whichm not considering the reheating of the fluid, increased from 43.1% to 54.9% when the temperature increased from 700 °C up to 1300 °C (Figure 4a). Higher temperatures at the turbine inlet indeed resulted in lower fluid densities, leading to increased power output extractable given the same pressure ratio across the machine. Increasing the turbine inlet temperature then is surely favorable due to the linear proportionality with the system efficiency.

Because of the higher energy output per unit of fluid processed and the constant volumes of the tanks (which depend on the cycle pressures that remain unchanged), the energy density of the plant increased from 9 kWh/m^3 up to 20 kWh/m^3 when the temperature increased from 700 °C to 1300 °C (no reheating, Figure 4b). The maximum energy density achieved was equal to 25 kWh/m^3 for a turbine inlet temperature of 1300 °C and considering two reheating stages (magenta line in Figure 4b). This value is lower than vanadium batteries.

The fuel consumption per unit of energy released can also be lowered by increasing the turbine inlet temperature since the energy-discharging process becomes more efficient (Figure 4c). In particular, when the turbine was designed to operate at a temperature of 1300 °C without considering any reheater, and then the unitary fuel consumption of the plant decreased to 116 kg/MWh (blue line Figure 4c).

A further increase in roundtrip efficiency and therefore an additional reduction in fuel consumption can be obtained by including reheaters in the LCES plant layout. At 1300 °C, considering one reheater can increase the roundtrip efficiency of the plant from 54.9% to 56.9% and reduce the fuel consumption from 116 kg/MWh down to 114 kg/MWh (Figure 4a,c). A second reheating stage can further improve the efficiency by up to 57.5% and decrease the fuel consumption to 113 kg/MWh (Figure 4a,c). Increasing reheating stages also allows increasing the energy density of the plant owing to the higher energy output generated per unit of fluid stored (Figure 4b). Compared to a conventional gas turbine, this system allows a substantial increase (approximately 35%) in thermal efficiency because the compression process is realized with the stored renewable energy, and therefore lower fuel consumption.

It is possible to notice, however, that the introduction of additional reheaters leads to lower incremental increases in performance. While the introduction of a reheating stage led to a 4.3% of efficiency improvement, the second one allowed achieving only a 1.4% increase, which may not be sufficient to justify the increase in cost and complexity associated.

An important variable is also the discharge time achievable from the LCES plant. Given that the charging time of the unit was fixed to 8 h and the power available in case of discharge was also fixed to 50 MW, by optimizing the plant parameters, it is possible to extend the duration time in which the unit would be available to supply power to utilities. Longer discharge times indeed make the energy storage system more flexible in responding to more prolonged shortages or decreases in power supply provided by RES (for instance caused by a reduced availability of solar radiation or wind speed). In this case, the increase of the turbine inlet temperature also allowed extending the discharge time of the unit from 14.6 h, at 1000 °C, and with no reheating, up to 18.2 h at 1300 °C and with no reheating. Including one or two reheaters in the layout would lead to an increase in the discharge time of 1.2 h and 2.2 h, respectively (Figure 4d). This discharge time is in the same order of magnitude as the time period in which solar energy is not available.

Besides being an important design parameter, the temperature at the turbine inlet, controlled by the mass flow rate of fuel injected in the combustor, could be an effective control variable to regulate the discharge of the LCES plant. A temperature reduction would shorten the duration time and therefore fasten the discharging of the plant by increasing the mass flow rate of stored CO_2 processed. An increase in the turbine inlet temperature would elongate the discharge time to provide additional power supply for longer times if needed.

Figure 5 analyzes the effect of the maximum pressure achieved in the plant on the aforementioned performance indicators. Figure 5a shows the low dependency of the roundtrip efficiency from the maximum design pressure of the plant, remaining almost constant when the pressure at which the CO_2 is stored at the end of the charging cycle varies from 125 bar to 250 bar. The positive effect of having lower pressure at the turbine inlet and therefore lower density is indeed counterbalanced by a reduced pressure ratio across the machine, which decreases the energy output extractable by the expansion of the fluid per unit of thermal energy input received.

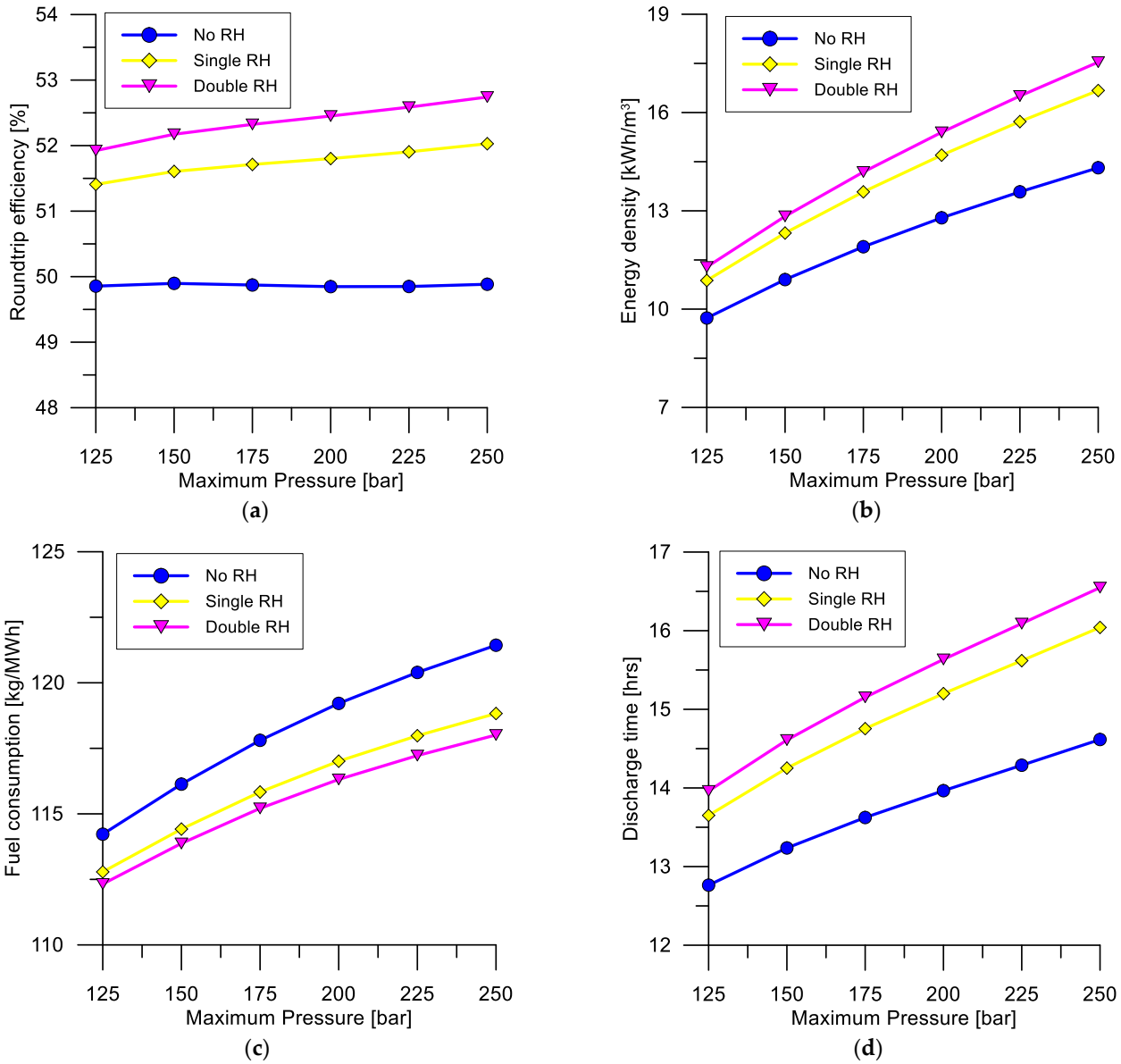

Figure 5. Effect of the maximum pressure and number of reheaters (RH) on the LCES system roundtrip efficiency (**a**), energy density (**b**), fuel consumption during a discharge cycle (**c**), and discharge time (**d**).

This means that, from an efficiency standpoint, decreasing the maximum pressure would be beneficial as it would allow decreasing the capital and operational expenditures, lifted up by safety and material requirements needed when dealing with components operating at higher pressures.

However, the maximum design pressure of the system directly impacts the energy density of the plant, which decreased from 15 kWh/m^3 for a pressure of 250 bar down to

approximately 10 kWh/m^3 for a pressure of 125 bar. In fact, liquefying the CO_2 at lower pressures at the end of the charging cycle caused lower densities, and therefore larger tank volumes required for the working fluid storage.

The energy density of the plant can however be increased by considering one or two reheating stages in the layout, raising it to 12 kWh/m^3 and 13 kWh/m^3 with the introduction of one or two reheating stages, respectively, when the CO_2 is stored at a maximum pressure of 125 bar (Figure 5b).

The maximum pressure of the system also affects the fuel consumption of the plant. Indeed, decreasing the maximum pressure of the system from 250 bar down to 125 bar allowed a decrease in the fuel consumption from 121 kg/MWh to 115 kg/MWh (Figure 5c). A further reduction is possible by considering one or two reheaters, which can drop the fuel consumption to approximately 113 kWh/MWh (Figure 5c). This is due to a more efficient regeneration that allows the CO_2 to flow into the indirect combustor at higher temperatures, reducing the need for fuel input.

The discharge time also decreased to 12.7 h when the maximum pressure was lowered to 125 bar (Figure 5d) since less fluid can be stored in the high-pressure CO_2 storage tanks. By introducing a reheating stage, at 125 bar the discharge time can be increased to 13.6 h, and approximately 14 h with a second reheating stage (Figure 5d).

The results then showed that when choosing the maximum pressure of the LCES system in the design stage, a trade-off exists in terms of system and components' costs. Higher pressures lead to reduced volumes required to store the fluid but more strict safety procedures and more performant materials. Lower pressures require larger storage tanks, but more off-the-shelf components and reduced operational expenditures due to lower fuel consumption. A detailed cost analysis should guide the decision-making process on such design parameters. Moreover, increasing the system pressure to 250 bar allows us to achieve a discharge time of approximately 16 h, which is approximately the same period of non-availability of solar energy.

The effect of the variation of the system discharge pressure on the system efficiency and energy density is displayed in Figure 6a,b. Lowering the discharge pressure of the system allows having a higher pressure ratio across the turbine and therefore greater power output in the discharging phase. For this reason, the roundtrip efficiency increased from 44.0% up to 54.0% when the discharge pressure was lowered from 40 bar down to 10 bar (no reheating, Figure 6a).

As a drawback, the energy density of the plant decreased from 15 kWh/m^3 to 8 kWh/m^3 for the same pressure decrease (Figure 6b). What causes this large drop is the increased tank volumes required for the storage of large amounts of methanol required to condensate back the CO_2 under liquid form at the end of the discharging cycle. Indeed, when the discharge pressure of the CO_2 was decreased, the condensation temperature decreased as well and became closer to the evaporation temperature at the beginning of the charging cycle. The smaller temperature differential between the evaporation (at 5.2 bar) and the condensation (at 10 bar) requires excessively increasing the mass flow rate of methanol used as a heat sink and, in turn, the tank volume needed for the storage.

Because of the greater efficiency, fuel consumption also decreased to 117 kg/MWh for a discharge pressure of 10 bar (Figure 6c). Owing to a larger energy output per unit of fluid processed, the duration of the discharging phase also increased to 17.8 h when the discharge pressure was lowered to 10 bar (no reheating, Figure 6d).

The only limiting factor in lowering the discharge pressure is represented by the large mass of methanol required as a "cold battery" to liquefy the CO_2 at a temperature lower than the ambient one. One possible technical solution to overcome this problem could be the adoption of a tank containing a cryogenic phase change material with a melting temperature between −56 °C and −40 °C. This would allow the replacement of the methanol a coolant, reducing the tank storage volumes required and therefore increasing the LCES performance and energy density.

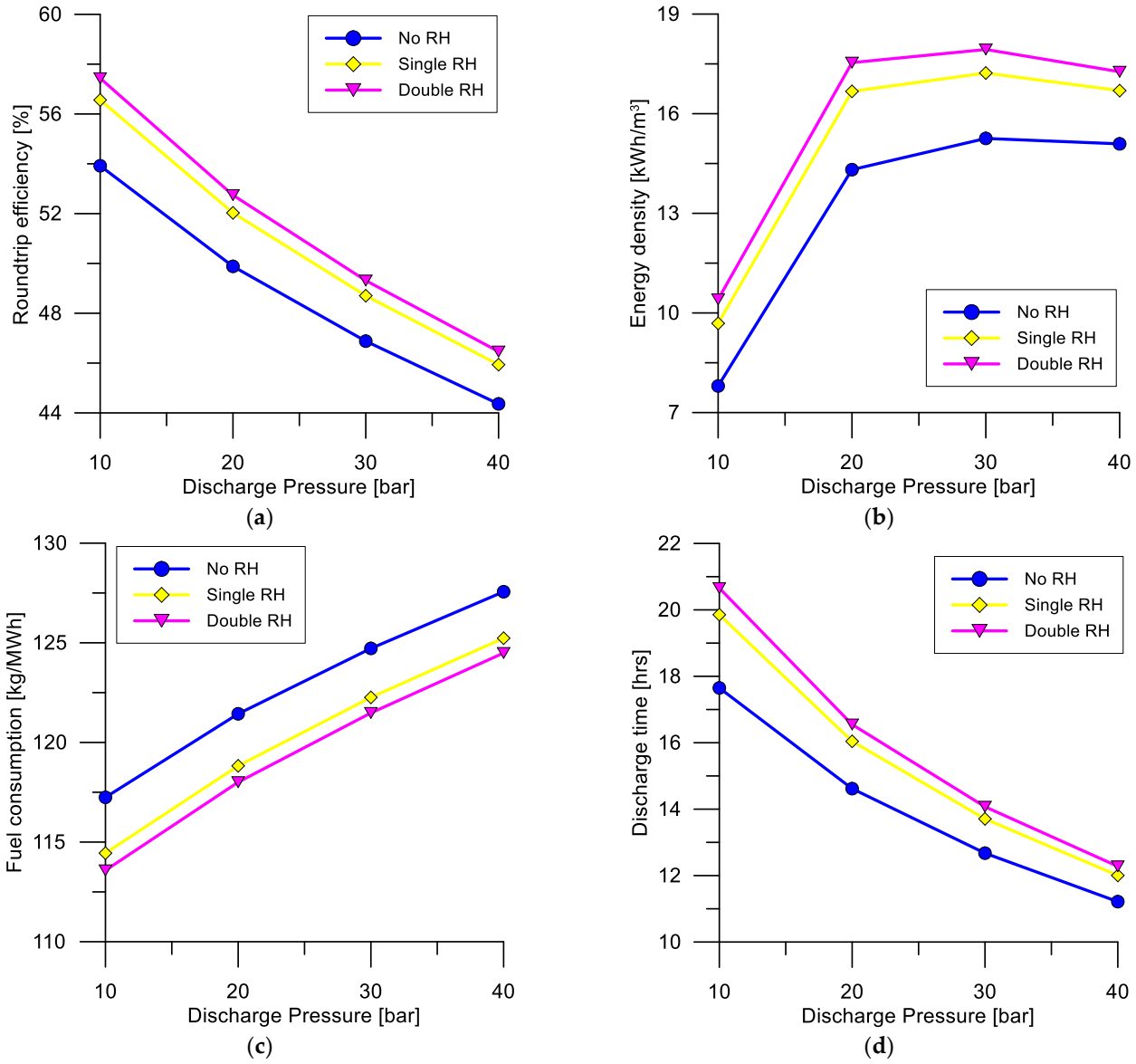

Figure 6. Effect of the discharge pressure and number of reheaters (RH) on the LCES system roundtrip efficiency (**a**), energy density (**b**), fuel consumption during a discharge cycle (**c**), and discharge time (**d**).

5. Conclusions

The research presented a rigorous thermodynamic study of a LAES and LCES system. The analysis considered an advanced configuration for the LAES unit and a novel layout for the LCES one. The comparison showed that LCES systems can achieve higher roundtrip efficiencies than LAES, i.e., 50.0% against 46.3%, a lower exergy destruction per unit of energy released, i.e., 0.80 MWh/MWh versus 0.91 MWh/MWh, and lower fuel consumption per unit of energy discharged, i.e., 121 kg/MWh against 205 kg/MWh for the LAES case. However, the LAES system showed greater energy density, i.e., 21 kWh/m^3 against 15 kWh/m^3 of the LCES system in its basic layout and design configuration. To further optimize the performance of the LCES unit and increase the energy density, a parametric analysis was carried out on the main design thermodynamic variables and layout arrangements of the LCES system.

The main findings included the following:

- The increase of the turbine inlet temperature is beneficial from an efficiency and energy density point of view. Increasing the temperature at the turbine inlet up to 1300 °C can increase the round-trip efficiency to 54%, decrease the fuel consumption to 117 kg/MWh, and increase the energy density to 21 kWh/m^3, comparable to the one of the LAES system. The turbine inlet temperature was also revealed to be an effective control variable for the regulation of the energy storage plant since it allows shortening or elongating the duration time of the system discharging phase;
- More reheatings are always beneficial for the system performance because it improves the efficiency of the expansion during the discharging phase and causes a better utilization of the fuel. However, the progressively lower incremental advantage derived from the introduction of a second reheating stage may not justify the increase in complexity and cost associated with its adoption;
- The maximum design pressure of the system did not affect the roundtrip efficiency of the unit. Lowering it to 125 bar may lead to advantages in terms of reduced fuel consumption (down to 110 kg/MWh considering one reheating stage) as well as lower costs for safety equipment and more off-the-shelf components. However, lower pressure leads to a lower energy density for the LCES unit, with the consequent disadvantage of the requirement of larger volumes for the storage tanks. A cost analysis should guide the decision-making process in such a trade-off;
- Having lower discharge pressure can be beneficial for the system roundtrip efficiency, discharge time, and fuel consumption, but the large amount of methanol required to condensate the CO_2 at the end of the discharge cycle at pressures lower than 10 bar may lead to unsustainable capital expenditures required for excessive methanol storage tank volumes;
- The long discharge times achievable with LCES technology represent a strong advantage in terms of system operational flexibility, allowing it to respond to prolonged fluctuations in RES power supply.

Because the energy storage systems taken into account in the analysis consider the input of additional energy input to extend the duration of the discharge phase and to improve the efficiency of the overall discharge process, future work will consider the replacement of such additional thermal energy input as well as a more comprehensive analysis related to assess the possible role of energy storage technologies in nuclear power applications.

Author Contributions: Conceptualization, R.C. and M.M.; methodology, M.M.; software, M.M.; formal analysis, M.M. and R.C.; investigation, M.M.; resources, R.C.; data curation, M.M. and R.C.; writing—original draft preparation, M.M.; writing—review and editing, R.C.; visualization, M.M.; supervision, R.C.; project administration, M.M. and R.C.; funding acquisition, R.C. All authors have read and agreed to the published version of the manuscript.

Funding: This research received no external funding.

Data Availability Statement: Not applicable.

Acknowledgments: The authors would like to acknowledge the support from Vittorio Tola and Giorgio Cau during the drafting of this manuscript.

Conflicts of Interest: The authors declare no conflict of interest.

Nomenclature

Symbols:

η	Efficiency	[%]
h	Enthalpy	[kJ/K]
$\dot{m}$	Mass flow rate	[kg/s]
p	Pressure	[bar]
s	Entropy	[kJ/K]
t	Time	[s]
x	Quality	[-]

CND	Condenser
CO_2	Carbon dioxide
COOL	Cooler
CO_2	Carbon dioxide
COOL	Cooler
COP	Coefficient Of Performance
EV	Evaporator
FT	Flash Tank

$\dot{E}$	Exergy flow	[kW]	G	Generator	
$\dot{I}$	Exergy destruction rate	[kW]	HTM	High-Temperature tank (Methanol)	
PR	Pressure Ratio	[-]	HTP	High-Temperature tank (Propane)	
T	Temperature	[°C]	HX	Heater	
$\dot{W}$	Power	[kW]	IC	Intercooler	
			L	Liquid	
Subscripts:			LAES	Liquid Air Energy Storage	
ch	Charging		LCES	Liquid Carbon Dioxide Energy Storage	
cs	Cold side		LT	Liquid Air Tank	
disch	Discharging		LTM	Low-Temperature tank (Methanol)	
el	Electric		LTP	Low-Temperature tank (Propane)	
hs	Hot side		M	Motor	
in	Inlet		MX	Mixer	
m	Mechanical		ORC	Organic Rankine Cycle	
max	Maximum		PHES	Pumped-Hydro Energy Storage	
min	Minimum		PMP	Pump	
out	Outlet		PTES	Pumped-Thermal Energy Storage	
pmp	Pump		REG	Regenerator	
0	total		RES	Renewable Energy Source	
			RH	Reheater	
Acronyms:			RT	Roundtrip efficiency	
C	Compressor		SH	Superheater	
CAES	Compressed Air Energy Storage		T	Turbine	
CB	Coldbox		TMS	Thermo-Mechanical Energy Storage	
CC	Combustor		TRL	Technological Readiness Level	
CCES	Compressed Carbon dioxide Energy Storage		V	Vapor	
CH_4	Methane		VLV	Expansion Valve	

References

1. Kim, J.H.; Alameri, S.A. Harmonizing nuclear and renewable energy: Case studies. *Int. J. Energy Res.* **2020**, *44*, 8053–8061. [CrossRef]
2. Kim, J.H.; Song, M.M.; Alameri, S.A. Emerging areas of nuclear power applications. *Nucl. Eng. Des.* **2019**, *354*, 110183. [CrossRef]
3. DIng, W.; Sheng, Q.; Zhang, J.; Zhu, X. Flow battery: An energy storage alternative for hydropower station. In Proceedings of the 2021 3rd International Academic Exchange Conference on Science and Technology Innovation IAECST 2021, Guangzhou, China, 10–12 December 2021; pp. 1869–1876. [CrossRef]
4. Rahman, M.A.; Kim, J.H.; Hossain, S. Recent advances of energy storage technologies for grid: A comprehensive review. *Energy Storage* **2022**, *4*, e322. [CrossRef]
5. Shiva Kumar, S.; Lim, H. An overview of water electrolysis technologies for green hydrogen production. *Energy Rep.* **2022**, *8*, 13793–13813. [CrossRef]
6. Borri, E.; Tafone, A.; Romagnoli, A.; Comodi, G. A review on liquid air energy storage: History, state of the art and recent developments. *Renew. Sustain. Energy Rev.* **2021**, *137*, 110572. [CrossRef]
7. Mahfoud, R.J.; Alkayem, N.F.; Zhang, Y.; Zheng, Y.; Sun, Y.; Alhelou, H.H. Optimal operation of pumped hydro storage-based energy systems: A compendium of current challenges and future perspectives. *Renew. Sustain. Energy Rev.* **2023**, *178*, 113267. [CrossRef]
8. Hamiche, A.M.; Stambouli, A.B.; Flazi, S.; Koinuma, H. Compressed air storage: Opportunities and sustainability issues. *Energy Storage*, 2023, *early view*. [CrossRef]
9. Liang, T.; Vecchi, A.; Knobloch, K.; Sciacovelli, A.; Engelbrecht, K.; Li, Y.; Ding, Y. Key components for Carnot Battery: Technology review, technical barriers and selection criteria. *Renew. Sustain. Energy Rev.* **2022**, *163*, 112478. [CrossRef]
10. Dumont, O.; Lemort, V. Pumped Thermal Energy Storage Based on ORC. In *Encyclopedia of Energy Storage*; Elsevier: Oxford, UK, 2022; pp. 68–78. [CrossRef]
11. Dumont, O.; Frate, G.F.; Pillai, A.; Lecompte, S.; De Paepe, M.; Lemort, V. Carnot battery technology: A state-of-the-art review. *J. Energy Storage* **2020**, *32*, 101756. [CrossRef]
12. McTigue, J.; Farres-Antunez, P.; Ellingwood, K.; Phys Lett, A.; Neises, T.; White, A. Pumped thermal electricity storage with supercritical CO_2 cycles and solar heat input. *AIP Conf. Proc.* **2020**, *2303*, 190024. [CrossRef]
13. Novotny, V.; Basta, V.; Smola, P.; Spale, J. Review of Carnot Battery Technology Commercial Development. *Energies* **2022**, *15*, 647. [CrossRef]
14. Frate, G.F.; Ferrari, L.; Desideri, U. Rankine carnot batteries with the integration of thermal energy sources: A review. *Energies* **2020**, *13*, 4766. [CrossRef]

15. Smith, E.M. Storage of electrical energy using supercritical liquid air. *Inst. Mech. Eng. (Lond.) Proc.* **1977**, *191*, 289–298. [CrossRef]
16. Vecchi, A.; Li, Y.; Ding, Y.; Mancarella, P.; Sciacovelli, A. Liquid air energy storage (LAES): A review on technology state-of-the-art, integration pathways and future perspectives. *Adv. Appl. Energy* **2021**, *3*, 100047. [CrossRef]
17. O'Callaghan, O.; Donnellan, P. Liquid air energy storage systems: A review. *Renew. Sustain. Energy Rev.* **2021**, *146*, 111113. [CrossRef]
18. Ji, W.; Chen, L.B.; Guo, L.N.; Xu, H.; An, B.L.; Wang, J.J. Theoretical investigation of a closed liquid CO_2 energy storage system. *IOP Conf. Ser. Mater. Sci. Eng.* **2020**, *755*, 012022. [CrossRef]
19. Sun, L.; Tang, B.; Xie, Y. Performance assessment of two compressed and liquid carbon dioxide energy storage systems: Thermodynamic, exergoeconomic analysis and multi-objective optimization. *Energy* **2022**, *256*, 124648. [CrossRef]
20. Angelino, G. Real gas effects in carbon dioxide cycles. In Proceedings of the ASME 1969 Gas Turbine Conference and Products Show, Cleveland, OH, USA, 9–13 March 1969.
21. Marchionni, M.; Bianchi, G.; Tassou, S.A. Review of supercritical carbon dioxide (sCO_2) technologies for high-grade waste heat to power conversion. *SN Appl. Sci.* **2020**, *2*, 611. [CrossRef]
22. Astolfi, M.; Rizzi, D.; Macchi, E.; Spadacini, C. A Novel Energy Storage System Based on Carbon Dioxide Unique Thermodynamic Properties. In Proceedings of the ASME Turbo Expo 2021: Turbomachinery Technical Conference and Exposition, Virtual, 7–11 June 2011; p. 4. [CrossRef]
23. Tang, B.; Sun, L.; Xie, Y. Comprehensive performance evaluation and optimization of a liquid carbon dioxide energy storage system with heat source. *Appl. Therm. Eng.* **2022**, *215*, 118957. [CrossRef]
24. Cao, Z.; Deng, J.; Zhou, S.; He, Y. Research on the feasibility of compressed carbon dioxide energy storage system with underground sequestration in antiquated mine goaf. *Energy Convers. Manag.* **2020**, *211*, 112788. [CrossRef]
25. Bartela, Ł.; Skorek-Osikowska, A.; Dykas, S.; Stanek, B. Thermodynamic and economic assessment of compressed carbon dioxide energy storage systems using a post-mining underground infrastructure. *Energy Convers. Manag.* **2021**, *241*, 114297. [CrossRef]
26. Xu, M.; Wang, X.; Wang, Z.; Zhao, P.; Dai, Y. Preliminary design and performance assessment of compressed supercritical carbon dioxide energy storage system. *Appl. Therm. Eng.* **2021**, *183*, 116153. [CrossRef]
27. Bell, I.H.; Wronski, J.; Quoilin, S.; Lemort, V. Pure and pseudo-pure fluid thermophysical property evaluation and the open-source thermophysical property library coolprop. *Ind. Eng. Chem. Res.* **2014**, *53*, 2498–2508. [CrossRef]
28. Krawczyk, P.; Szabłowski, Ł.; Karellas, S.; Kakaras, E.; Badyda, K. Comparative thermodynamic analysis of compressed air and liquid air energy storage systems. *Energy* **2018**, *142*, 46–54. [CrossRef]
29. Marchionni, M.; Bianchi, G.; Tassou, S.A. Techno-economic assessment of Joule-Brayton cycle architectures for heat to power conversion from high-grade heat sources using CO_2 in the supercritical state. *Energy* **2018**, *148*, 1140–1152. [CrossRef]
30. Stathopoulos, P. Comprehensive Thermodynamic Analysis of the Humphrey Cycle for Gas Turbines with Pressure Gain Combustion. *Energies* **2018**, *11*, 3521. [CrossRef]
31. Awbery, J.H. A new process for liquefying air. *Nature* **1941**, *148*, 14. [CrossRef]
32. Allam, R.; Martin, S.; Forrest, B.; Fetvedt, J.; Lu, X.; Freed, D.; William Brown, G., Jr.; Sasaki, T.; Itoh, M.; Manning, J. Demonstration of the Allam Cycle: An Update on the Development Status of a High Efficiency Supercritical Carbon Dioxide Power Process Employing Full Carbon Capture. *Energy Procedia* **2017**, *114*, 5948–5966. [CrossRef]